JOURNAL OF MATERIALS SCIENCE 17 (1982) 1930–1938

Hydrogen trapping phenomena in carbon steel

W. Y. CHOO*, JAI YOUNG LEE
Department of Materials Science, Korea Advanced Institute of Science and Technology, P.O. Box 150, Cheongyangni, Seoul, Korea

Hydrogen trapping phenomena in carbon steel with different amounts of trapping sites were investigated by thermal analysis and permeation experiments. In thermal analysis, the relative amount of trapped hydrogen and the activation energy for evolution from various lattice defects were calculated by monitoring the pressure change caused by the release of hydrogen from hydrogen-charged specimens heated at a uniform rate. Hydrogen release peaks were observed at 116, 205 and 387° C, respectively, when the hydrogen-charged specimens with various defects were heated at a constant heating rate of 2.6° C min^{-1}. Analysis suggested that the peak at 116° C corresponded to release from ferrite–cementite interfaces and the peak at 205° C corresponded to release from dislocations. The activation energy for evolution of trapped hydrogen determined experimentally from the measured peak temperature at different heating rates was found to be 18.4 kJ mol^{-1} in the ferrite–cementite interface. The hydrogen energy level around the trapping site was suggested from the trap activation energy and expected saddle-point energy. It was observed that most of the hydrogen is trapped in dislocations in spheroidized 0.49 wt% carbon steel.

1. Introduction

The hydrogen solubility in iron and steel increases as temperature increases. Iron and steel may pick up hydrogen during the heat treatment process and hydrogen causes embrittlement of iron and steel. The hydrogen embrittlement problem is specially severe in low alloy high-strength steel, which is in great demand in modern industry. In order to cope with this embrittlement problem in iron and steel, many researchers have studied the Fe–H system [1–3] and found that a certain amount of hydrogen must move to the crack-tip area to cause embrittlement. Therefore, it is very important to solve and understand the problem of hydrogen embrittlement in iron and steel.

Fig. 1 shows that the diffusivity of hydrogen in iron deviates markedly from that predicted by extrapolation of high-temperature data taken below 300° C [4–10]. The apparent activation energy in this low-temperature region is in the range of 36 to 48 kJ mol^{-1}, while that in the higher-temperature region is 12 to 20 kJ mol^{-1}. Many researchers [11–17] believe that these phenomena take place due to hydrogen trapping in the lattice defects of iron and steel (dislocations, microvoids, grain boundary and interface defects) at low temperatures, as the trapping sites have lower energy level than normal lattice sites.

Pressouyre [11] has classified types of trapping sites by their physical nature for hydrogen in iron and has suggested that vacancy, alloying element, dislocation, interface and microvoid are possible trapping sites.

Analysing the hydrogen diffusivity data in iron, Oriani [12] has estimated the trap density and trap–hydrogen interaction energy and has claimed that interfaces and microvoids are major trapping sites in steels which are not cold-worked. Kumnick *et al.* [13] have concluded that dislocation and dislocation debris are trapping sites for hydrogen in their research of hydrogen permeation in cold-worked steel. Riecke [14] has also found that dis-

*Present address: Department of Metallurgy and Materials Science, Carnegie-Mellon University, Pittsburg, PA 15213, USA.

0022–2461/82/071930–09$03.58/0

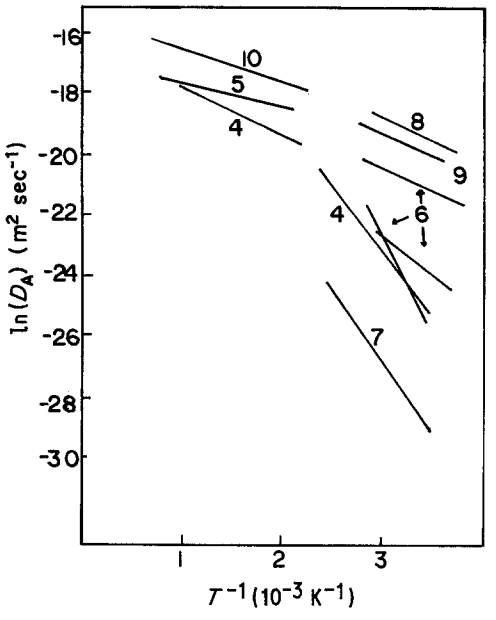

Figure 1 Representative data for the apparent diffusivity of hydrogen in iron and ferritic steel.

locations and dislocation pile-ups act as trapping sites in the measurement of the hydrogen diffusivity of hydrogen-charged cold-worked and recrystallized iron specimens. Pressouyre *et al.* [15] have found that TiC particles trap hydrogen irreversibly. In this study, they have applied the permeation transients method. As a basic work, Wada *et al.* [16] have observed the change of specific heat through the first-order phase transformation at 13.7 K in the hydrogen–iron system and have verified that hydrogen is trapped in microvoids as gas molecules. Kotyc *et al.* [17] have argued that the ferrite–cementite interface is the dominant type of trapping site in carbon steel, deduced from their measurements of the dependence of hydrogen diffusivity on the amount of ferrite–cementite interface.

As described above, the anomalous behaviour of hydrogen diffusion in iron is claimed to be due to the hydrogen trapping in lattice defects. However, most of the experiments have been carried out with specimens containing all the kinds of defects without being able to isolate the effect of any one type of defect. This work is intended to control the interface area of ferrite–cementite of a specimen and analyse the hydrogen behaviour in the specimen by thermal analysis and the permeation technique to estimate the energy level around lattice defects in carbon steel.

It is also hoped that an analysis of the above data will provide a greater understanding of hydrogen trapping phenomena in carbon steel.

2. Theory

2.1. Thermal analysis

If the energy level of hydrogen near the trapping site is known, the rate of hydrogen escape from the trapping site can be estimated. However, the energy level of the hydrogen around the trapping site is not known. In this work, the energy level of hydrogen around the defect site is estimated by thermal analysis of the trapped hydrogen. The saddle-point energy of the trapping site, E_s, and the activation energy in the normal lattice, E_{aD}, are assumed to be different energy states, as in Fig. 2. The trap reaction of hydrogen in trapping site is expressed as

$$\text{H}_{\text{trap}} \rightleftharpoons \square_{\text{trap}} + \text{H}_{(\text{in lattice})}, \qquad (1)$$

where $\square_{\text{trap}}$ is the trapping site.

The rate of hydrogen escape from the trapping site in Equation 1 is expressed as [18]

$$\frac{dX_T}{dt} = A(1 - X_T)\exp(-E_{aT}/RT), \qquad (2)$$

where $X_T = (C_{x0} - C_{xt})/C_{x0}$ and C_{x0} is the hydrogen concentration in the trapping site at $t = 0$, C_{xt} is the hydrogen concentration in the trapping site at $t \neq 0$, R is the gas constant, T is the temperature and A is constant. Heating the hydrogen-charged specimen with uniform heating rate, ϕ, the rate of hydrogen escape, dX_T/dt, shows a maximum at a certain temperature, T_c,

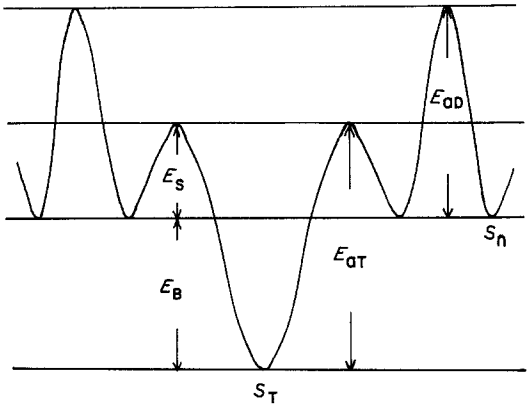

Figure 2 Model for trapping site. E_{aD}, diffusion activation energy of hydrogen in normal lattice; E_s, saddle-point energy; E_B, binding energy between trapping site and hydrogen; E_{aT}, trap activation energy; S_T, trapping site; and S_n, normal lattice site.

according to

$$\frac{d}{dt}\left(\frac{dX_T}{dt}\right) = \frac{dX_T}{dt}\left[\frac{E_{aT}}{T_c} - A\exp(-E_{aT}/RT_c)\right] = 0, \quad (3)$$

where A is a constant.

Taking the logarithm of Equation 3 and differentiating with respect to $(1/T_c)$ gives [19]

$$\frac{\partial \ln(\phi/T_c^2)}{\partial T^{-1}} = -E_{aT}/R. \quad (4)$$

Monitoring T_c at different heating rates, ϕ, trap activation energy, E_{aT}, can be calculated from Equation 4.

2.2. Estimation of trap parameter

The apparent hydrogen diffusivity, D_A, in iron and the permeation time-lag, t_1, has a relation [20] as

$$t_1 = \frac{a^2}{6D_A}, \quad (5)$$

where a is the thickness of the specimen. From this relation D_A can be estimated. McNabb and Foster [21] have derived an equation between t_1 and the lattice diffusivity, D_1, as

$$t_1 = \frac{a^2}{6D_1}(1+\alpha), \quad (6)$$

where $\alpha = N\mathscr{K}/p$, N is the trap density, $\mathscr{K}$ is the trapping rate and p is the detrapping rate. From Equations 5 and 6 it can be deduced that

$$D_1/D_A = 1 + \alpha. \quad (7)$$

After calculating the mean trap parameter, α, from Equation 7 the mean binding energy, E_B, of trapping site–hydrogen is obtained from the temperature dependence of α [22],

$$\alpha_{T_2}/\alpha_{T_1} = \exp\left(\frac{E_B}{R}(T_2^{-1} - T_1^{-1})\right), \quad (8)$$

where α_{T_1} and α_{T_2} are the mean trap parameters at T_1 and T_2, respectively, for the same specimen.

Since various kinds of trapping sites exist in the specimen, the mean trap parameter, α, in Equation 7 includes all the effects of various kinds of trapping sites. One cannot single out the effect of one type of trapping site and hydrogen interaction from the mean trap parameter, α, obtained from one type of specimen. However, if two specimens have the same types of trapping sites except for one type, the effect on hydrogen of one type of trapping site can be obtained from the difference of the mean trap parameters, α, of the two kinds of specimens. Let α_{1s1} be the mean trap parameter due to all the types of trapping sites–hydrogen interactions of Specimen 1, α_{1s2} be the mean trap parameter of Specimen 2, which is made having only one type of trapping site different from Specimen 1 and let α_2 be the difference between α_{1s1} and α_{1s2}. The trap parameter, α_2, only includes the effect of one kind of trapping site. The difference of permeation time lag, t_{1_1} and t_{1_2}, of Specimens 1 and 2, respectively, is given from Equation 6 as

$$t_{1_2} - t_{1_1} = \frac{a^2}{6D_1} \cdot \alpha_2. \quad (9)$$

From Equation 9, α_2, which represents only the effect of one type of defect–hydrogen interaction can be calculated. Combining α_2 and Equation 8, the binding energy of one type of trapping sites and hydrogen is obtained [22].

3. Experimental procedure

3.1. Sample preparation

Electrolytic iron and graphite were melted in an induction furnace to make a carbon steel ingot. This ingot was remelted in VAR to remove the gas elements in the sample. The chemical composition of specimen is shown in Table I. After forging at 1150° C, the ingot was normalized for 2 h at 900° C. The amount of ferrite–cementite interface area is controlled by spheroidizing heat-treatment. The specimens for thermal analysis were in cylindrical shape, 8 mm in diameter and 15 mm in height. The specimens for permeation experiments were disc-shaped, 40 mm in diameter and 0.2 to 0.75 mm in thickness.

TABLE I Chemical composition of specimen

Specimen	Elements (wt ppm)							
	C	N	S	P	Ni	Cr	Si	Mn
Electrolytic iron	50	–	50	40	–	–	–	50
0.12 wt% carbon steel	1260	50	12	–	411	–	–	–
0.49 wt% carbon steel	4941	68	12	–	509	–	–	–

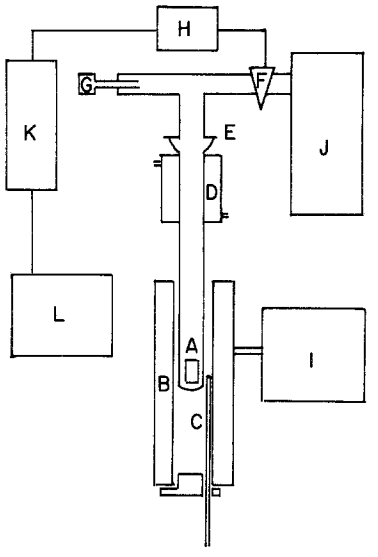

Figure 3 Schematic diagram of hydrogen thermal analysis apparatus. Showing: A, specimen; B, furnace; C, thermocouple; D, water-jacket; E, ball-and-socket joint; F, pneumatic vacuum solenoid valve; G, vacuum senser; H, governor; I, temperature programmer; J, vaccum pump; K, vacuum gauge; and L, recorder.

3.2. Experimental apparatus and methods

3.2.1. Thermal analysis

Cylindrical specimens were charged with hydrogen under 0.2 MPa hydrogen pressure at 400° C for 2 h, and then quenched into ice-water. The hydrogen-charged specimens were transferred to a reaction chamber (E in Fig. 3) and held under vacuum for 6 h at room temperature to remove mobile hydrogen, so only trapped hydrogen remained in the specimen. As each specimen was heated with a uniform heating rate, the trapped hydrogen started to evolve. The time of pressure change in reaction chamber between 10^{-4} and 5×10^{-1} Pa was checked and used to determine the hydrogen evolution rate from trapping sites. Pressure change is monitored by thermocouple gauge and chart-recorder. Blank test was carried out before each run to correct the pressure for leakage. The hydrogen evolution rate has been expressed by normalizing to a rate of 10, representing various rates from 10^{-4} to 5×10^{-1} Pa $min^{-1} g^{-1}$. The positions and heights of peaks in the evolution rate against temperature plot were assumed to be decided by the trap activation energy, E_{aT}, between hydrogen and trapping sites and the amount of hydrogen in trapping sites, respectively. As heating rates were increased, the positions of the peaks were moved towards the high-temperature side, as predicted by Equation 3. The activation energy of hydrogen evolution from trapping site was calculated by monitoring the change of peak position with variation of heating rates from 8.44 to 1.39° C min^{-1}.

3.2.2. Permeation experiment

The specimens with controlled amounts of defects were treated in a 0.2 MPa hydrogen atmosphere at 400° C in order to remove the surface impedance layer. Fig. 4 represents a schematic diagram of the permeation apparatus. To maintain high vacuum between specimen and reactor at high temperature, a copper "O"-ring was adopted. After setting the sample in the permeation apparatus, one side of reaction chamber (O in Fig. 4) was evacuated to 10^{-4} Pa and the other side of reaction chamber (P in Fig. 4) was held at 0.4 MPa hydrogen pressure. The permeation flux at a certain temperature, as a function of time, is measured monitoring the pressure change in the 10^{-4} Pa side of reaction chamber. The pressure gauge used was thermocouple gauge and chart-recorder. The experiment was continued until the flux reached steady-state. After the experiment, the specimen was heated to about 300° C, and the hydrogen was removed by evacuating both sides of the reaction

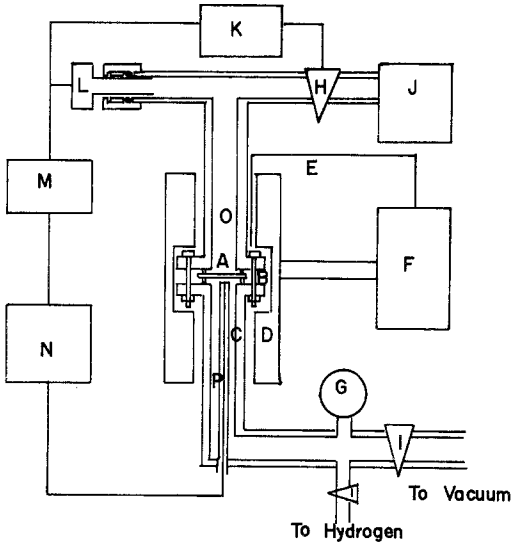

Figure 4 Schematic diagram of hydrogen permeation apparatus. Showing: A, specimen; B, copper "O"-ring; C, measuring thermocouple; D, furnace; E, controlling thermocouple; F, temperature controller; G, compound gauge; H, pneumatic vacuum solenoid valve; I, valve; J, mechanical and diffusion pump; K, governor; L, vacuum senser; M, vacuum gauge; N, recorder; O, reaction chamber; and P, pressure chamber.

chamber. The sample was then brought to a new temperature setting and the same procedure was repeated. The experimental temperature range was 130 to 250° C. The permeation time-lag method was adopted to calculate the hydrogen diffusivity from permeation rate data with variables of temperature, pressure and type of specimen.

4. Results

4.1. Thermal analysis

4.1.1. Relation between lattice defect and thermal analysis peak

A typical thermal analysis curve is shown in Fig. 5 for a heating rate of 2.6° C min^{-1}. After one cycle of thermal analysis, a second is done on the same sample. No peaks were observed, indicating that all the trapped hydrogen is evolved in the first cycle of analysis. In Fig. 5, three thermal analysis peaks are observed at 115, 205 and 387° C indicating that at least three types of trapping sites exist in carbon steel. The heights of each peak are different, indicating that the relative amount of hydrogen in each trapping site is different. Fig. 6 shows the microstructure of three different ferrite–cementite interface area specimens, Specimens a to c, which are used in this work. The ferrite–cementite interface area gradually decreases from Specimen a to Specimen c. Specimens a and c are heat-treated for 1 h at 920° C and air-cooled. After heat-treating for 10 min at 780° C, Specimen b is also heat-treated for 2 h at 705° C and air-cooled. Thermal analysis peaks for the three different ferrite–cementite area specimens at a heating rate of 2.6° C min^{-1} are shown in Fig. 7. As the ferrite–cementite interface area increases, only the heights of the peaks at 116° C increases. The heights of other peaks are not linearly increased as the ferrite–cementite interface area increases. It is concluded, therefore, that the peak at 116° C corresponds to hydrogen trapping in the ferrite–cementite interface. Three thermal analysis peaks are observed at 112, 215 and 305° C in pure iron at a heating rate of 2.6° C min^{-1} and the peak at 215° C corresponds to the dislocation–hydrogen interaction peak [19]. By comparing carbon steel data with pure iron data, it is expected that the thermal analysis peak at 205° C in carbon steel is due to interaction between the dislocation and hydrogen. The height of the 205° C peak in spheroidized carbon steel is much higher than that of the other carbon steel. The peak at 387° C appeared in thermal analysis, but no defect corresponding to this peak could be found.

4.1.2. Measurements of the trap activation energy

It is important to measure the trap activation energy, E_{aT}, in order to know the energy level around the trapping site. However, so far the trap activation energy, E_{aT}, has not been measured. In this work, the trap activation energy, E_{aT}, is obtained from Equation 4 by measuring the change of T_c at different heating rates, ϕ. These values are shown in Table II. The trap activation energy of the ferrite–cementite interface is 18.4 kJ mol^{-1} and this value is very close to the trap activation energy of the grain boundary in pure iron, 17.1 kJ mol^{-1} [19].

4.2. Permeation experiment

Fig. 8 shows the apparent hydrogen diffusivity

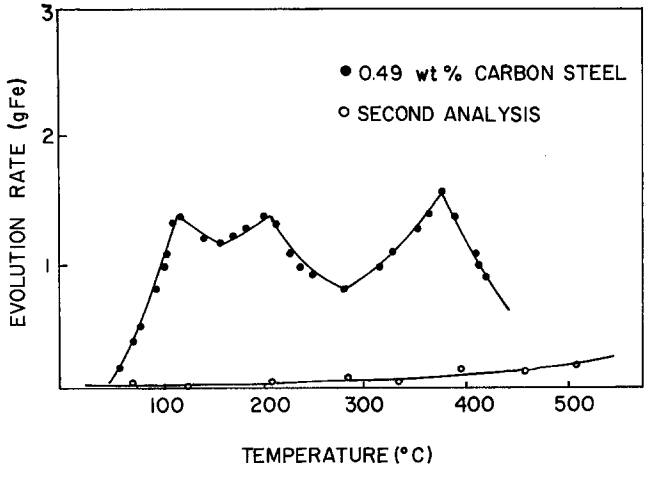

Figure 5 Typical thermal analysis peaks of hydrogen-charged carbon steel and second-analysis curve on the same sample.

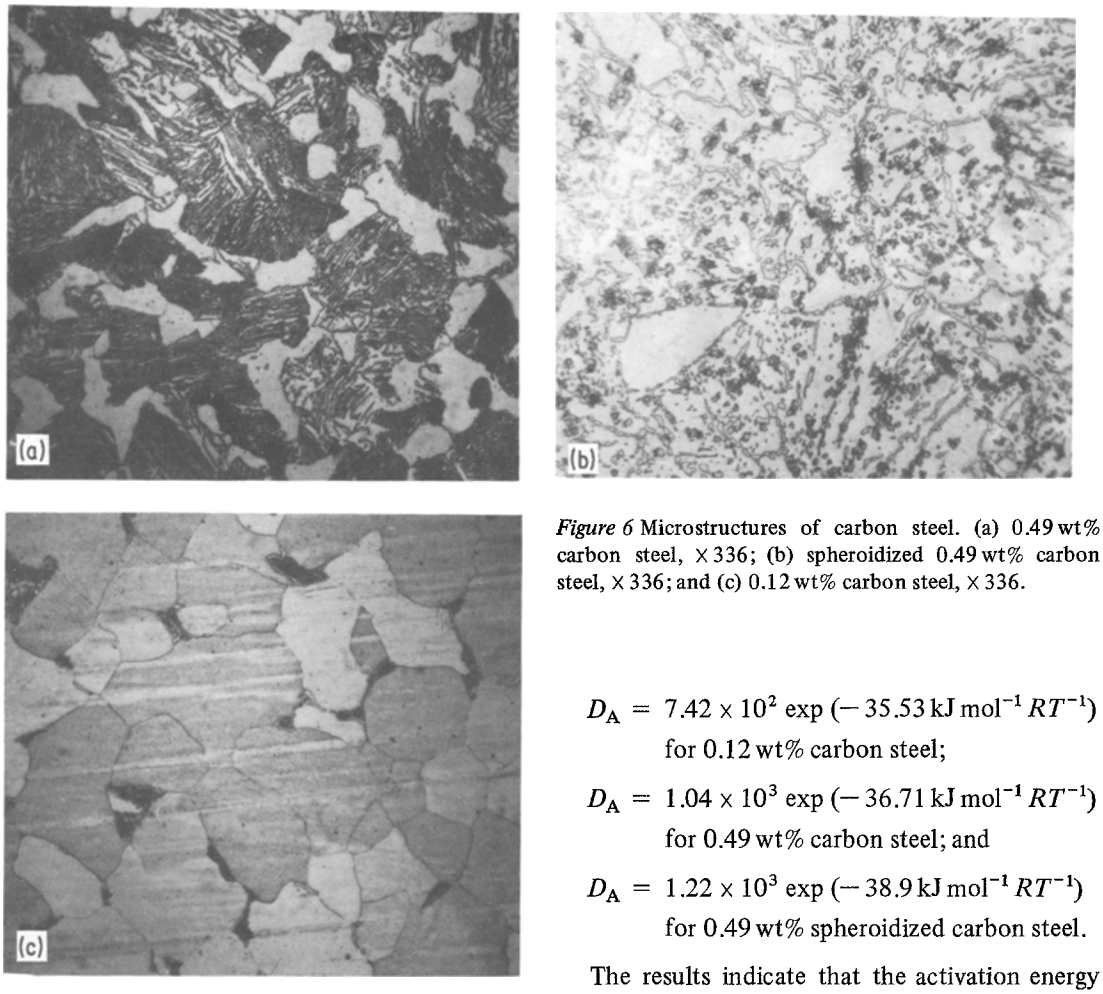

Figure 6 Microstructures of carbon steel. (a) 0.49 wt% carbon steel, × 336; (b) spheroidized 0.49 wt% carbon steel, × 336; and (c) 0.12 wt% carbon steel, × 336.

as a function of reciprocal temperature for specimens with different amounts of ferrite–cementite interface shown in Fig. 6. The least-square fit representative equations are as follows:

$$D_A = 7.42 \times 10^2 \exp(-35.53\,\text{kJ mol}^{-1} RT^{-1})$$
for 0.12 wt% carbon steel;

$$D_A = 1.04 \times 10^3 \exp(-36.71\,\text{kJ mol}^{-1} RT^{-1})$$
for 0.49 wt% carbon steel; and

$$D_A = 1.22 \times 10^3 \exp(-38.9\,\text{kJ mol}^{-1} RT^{-1})$$
for 0.49 wt% spheroidized carbon steel.

The results indicate that the activation energy difference between the 0.12 wt% carbon steel and the 0.49 wt% carbon steel is very small, and the activation energy is about 14 kJ mol^{-1} greater than that of pure iron, of 22.5 kJ mol^{-1} [22].

The mean trap parameter, α_1, accounts for

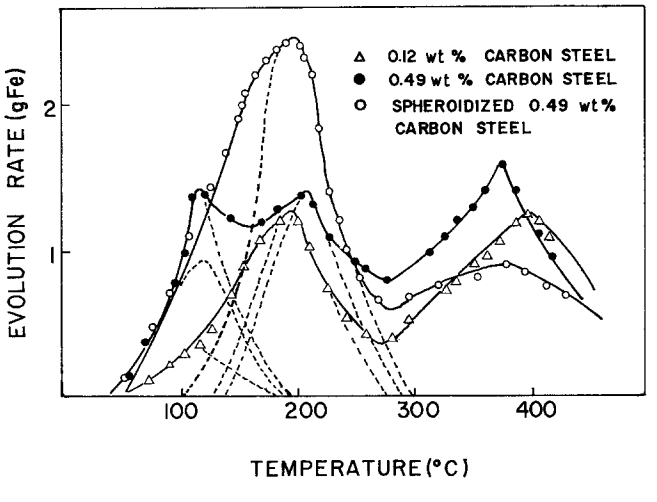

Figure 7 Dependence of the peak-heights on the amount of ferrite–cementite interface Heating rate: 2.6° C min^{-1}.

TABLE II Peak temperature of ferrite–cementite interface trapping site at various heating rates

Heating rate (° C min^{-1})	Peak temperature (° C)	Trap activation energy (kJ mol^{-1})
8.18	157	
5.44	137	
3.59	1.27	18.35
2.90	118	
1.47	73	

effects of all the types of trapping sites–hydrogen interactions in specimens which contain various types of trapping sites. α_1 can be calculated using Equation 6. In order to obtain α_1, a value of D_1 is needed. However, the values of D_1 so far reported vary quite widely [4, 23–25]. In this research a median value of the reported data for D_1 is taken to calculate α_1 as

$$D_1 = 2.24 \times 10^1 \exp(-16.8\,\text{kJ mol}^{-1} RT^{-1}).$$

Table III shows α_1 values obtained by Equation 6. The difference of mean trap parameter, α_2, between the 0.12 wt% carbon steel and the 0.49 wt% carbon steel describes the effect of the ferrite–cementite interface because the only difference between the two specimens is the amount of ferrite–cementite interface. These trap parameters, α_2, are given in Table IV. However, this value is small and the value at 250° C is positive, while the value of 50° C is negative. The binding energy of the ferrite–cementite interface–hydrogen, from the temperature dependence of these α_2 values cannot be calculated. The trap parameters, α_2, between the 0.49 wt% carbon steel and the spheroidized 0.49 wt% carbon steel are also given in Table IV. The binding energy of the trapping site–hydrogen calculated from the temperature dependence of α_2 is 26.06 kJ mol^{-1}. This value is almost the same as the binding energy of dislocation–hydrogen in pure iron, of 26.46 kJ mol^{-1} [19].

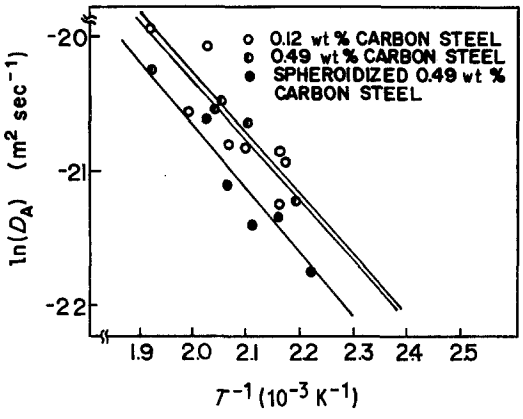

Figure 8 Temperature dependence of apparent hydrogen diffusivity in carbon steel.

5. Discussion

The thermal analysis peak attributed to ferrite–cementite occurs at 116° C when the specimen is heated at a rate of 2.6° C min^{-1}. The trap activation energy, E_{aT}, of the ferrite–cementite interface is 18.4 kJ mol^{-1} and this value is very close to the grain-boundary value of 17.1 kJ mol^{-1} [19]. This result indicates that the properties of the ferrite–cementite interface and the grain boundary against hydrogen are similar. It is necessary to know the energy level around the trapping site in order to understand the mechanism of hydrogen trapping and detrapping. In this work, an attempt is made to determine the energy level around the trapping site using the binding energy, E_B, of one-type trapping site and hydrogen, obtained from permeation experiments and trap activation energy, E_{aT}, estimated from thermal analysis of trapped hydrogen. It is impossible to calculate the binding energy of the ferrite–cementite interface–hydrogen using a permeation experiment, because the effect of hydrogen trapping in the ferrite–cementite interface is smaller than the trapping effect of other trapping sites (dislocations, etc.). However, it is assumed that saddle-point

TABLE III Temperature dependence of mean trap parameter, α_1, in carbon steel

Temperature (° C)	Specimen		
	0.12 wt% carbon steel	0.49 wt% carbon steel	Spheroidized 0.49 wt% carbon steel
250	1.206	1.065	1.916
200	2.474	2.344	3.980
150	5.088	5.070	8.555
100	11.399	11.926	21.350
50	30.479	33.788	68.102

TABLE IV Temperature dependence of trap parameter, α_2, in carbon steel

Temperature (° C)	Specimen	
	0.12 wt% carbon steel–0.49 wt% carbon steel	0.49 wt% carbon steel–spheroidized 0.49 wt% carbon steel
250	−0.1419	0.8509
200	−0.1297	1.6363
150	−0.0177	3.4852
100	0.5270	9.4241
50	3.3095	34.6204

energy, E_s, of the ferrite-cementite interface is almost the same as the value of the microvoids, 8 kJ mol^{-1} [19]. The expected energy level diagram is given in Fig. 9. This diagram implies that hydrogen moves into a trapping site easily at low temperature.

The binding energy of trapping site–hydrogen, calculated from the trap parameter, α_2, between 0.49 wt% carbon steel and spheroidized 0.49 wt% carbon steel is 26.06 kJ mol^{-1}. This value is almost the same as the binding energy of dislocation–hydrogen in pure iron, 26.46 kJ mol^{-1}. The position of the 205° C thermal analysis peak in carbon steel is almost the same as that of 215° C peak in pure iron which corresponds to the dislocation–hydrogen interaction peak. From the above two facts, the thermal analysis peak at 205° C corresponds to the dislocation–hydrogen interaction. In Fig. 7, the height of the thermal analysis peak at 205° C in spheroidized 0.49 wt% carbon steel is much higher than that of 0.49 wt% carbon steel and, in Fig. 8, the apparent hydrogen diffusivity, D_A, of speroidized 0.49 wt% carbon steel is smaller than the D_A value of the other carbon steel. The above two phenomena are explained by the increased dislocation density in spheroidized 0.49 wt% carbon steel. These results agree with the work of Sakamoto [26] which showed that the decrease of apparent hydrogen diffusivity in 430 stainless steel at room temperature is due to the increase of dislocation density which is caused by precipitated particles. The peak at 387° C is visible in the thermal analysis but at the present time we cannot determine which, if any, defect corresponds to this peak. If the major trapping site of hydrogen in carbon steel is known, the apparent hydrogen diffusivity in carbon steel can be estimated by controlling the amount of major trapping sites. In the thermal analysis, the height of the peak is related to the amount of hydrogen in the trapping site. Therefore, the major trapping site in carbon steel can be found using Fig. 7. Since the heights of the three thermal analysis peaks in 0.12 wt%, 0.49 wt% and spheroidized 0.49 wt% carbon steel are almost the same, the major trapping sites cannot be judged in this case. In the case of spheroidized 0.49 wt% carbon steel, the peak at 205° C is twice as high as for the others. Consequently, it is concluded that dislocations are the major trapping sites of hydrogen in spheroidized 0.49 wt% carbon steel.

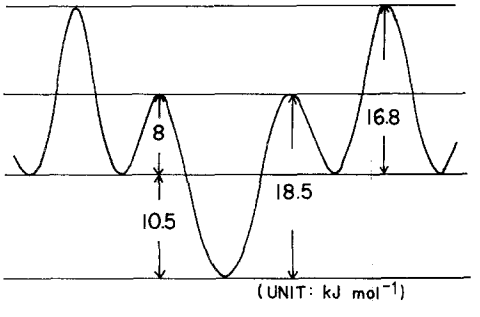

Figure 9 Energy level of hydrogen around the ferrite–cementite interface (compare with Fig. 2).

6. Conclusions

(a) The thermal analysis curve in carbon steel (evolution rate plotted against temperature) shows three peaks at 116, 205 and 387° C. The peak at 116° C corresponds to hydrogen release from the ferrite–cementite interfaces, and the peak at 205° C corresponds to hydrogen release from dislocations.

(b) The activation energy for hydrogen evolution from the ferrite–cementite interface is 18.4 kJ mol^{-1}.

(c) The energy level around the ferrite–cementite interface is suggested from the trap activation energy and the hydrogen–interface binding energy.

(d) The height of the thermal analysis peak at 205° C in spheroidized 0.49 wt% carbon steel is much higher than that in 0.49 wt% carbon steel, and the apparent hydrogen diffusivity, D_A, of spheroidized 0.49 wt% carbon steel is smaller

than the D_A value of other carbon steels. These two phenomena are interpreted to result from the increase of dislocation density in spheroidized 0.49 wt% carbon steel.

(e) It is suggested that the major type of trapping site of hydrogen is dislocations in spheroidized 0.49 wt% carbon steel.

Acknowledgement

The work was supported in part by a grant from the Korea Science and Engineering Foundation.

References

1. P. COTTERILL, *Prog. Mater. Sci.* **9** (1961) 201.
2. I. M. BERNSTEIN and A. W. THOMPSON, *Int. Met., Rev.* **212** (1976) 269.
3. M. CORNET and S. TALBOT-BESNARD, *Met. Sci.* **12** (1978) 335.
4. E. W. JOHNSON and M. L. HILL, *Trans. TMS AIME* **218** (1960) 1104.
5. T. HEUMAN and D. PRIMAS, *Z. Naturforsch* **21A** (1966) 260.
6. R. C. FRANK, D. E. SWERTS and D. L. FRY, *J. Appl. Phys.* **29** (1958) 892.
7. R. M. BARRER, *Trans. Faraday Soc.* **36** (1940) 1242.
8. W. BECK, J. D. M. BOCKRIS, J. McBREEN and L. NANIS, *Proc. Roy. Soc.* **A209** (1966) 220.
9. A. J. KUMNICK and H. H. JOHNSON, *Acta. Met.* **25** (1977) 891.
10. N. R. QUICK and H. H. JOHNSON, *ibid.* **26** (1978) 903.
11. G. M. PRESSOUYRE, *Met. Trans. A* **10A** (1979) 1571.
12. R. A. ORIANI, *Acta. Met.* **18** (1970) 147.
13. A. J. KUMNICK and H. H. JOHNSON, *Acta. Met.* **28** (1980) 33.
14. E. M. RIECKE in Proceedings of the 8th International Symposium on the Reactivity of Solids, Chalmers University of Technology, Goteborg, Sweden, June 1976, edited by J. Woode *et al.* (Plenum Press, New York, 1976) p. 361.
15. G. M. PRESSOUYRE and I. M. BERNSTEIN, *Met. Trans. A* **9A** (1978) 1571.
16. H. WADA and K. SAKAMOTO, *Scripta Met.* **13** (1979) 573.
17. M. KOTYLC and H. M. DAVIS, *Trans. ASM. Quart.* **53** (1961) 654.
18. H. E. KISSINGER, *Anal. Chem.* **29** (1957) 1702.
19. W. Y. CHOO and J. Y. LEE, *Met. Trans.* **13A** (1982) 135.
20. J. CRANK, "The Mathematics of Diffusion" (Clarendon Press, Oxford, 1975) p. 44.
21. A. McNABB and P. K. FOSTER, *Trans. TMS AIME* **227** (1963) 168.
22. W. Y. CHOO, KAIST PhD thesis, 1981, Seoul, Korea.
23. W. BANKOLOH and W. WENZEL, *Arch. Eisenhuttenw* **11** (1937) 273.
24. W. EICHENAUER, H. KUNZIG and W. PEBLER, *Z. Metalk.* **49** (1958) 220.
25. M. L. HILL and E. W. JOHNSON, *Trans. TMS AIME* **215** (1957) 717.
26. Y. SAKAMOTO and T. MASUMOTO, *Z. Metalk.* **63** (1977) 285.

Received 30 September
and accepted 26 November 1981